Juniper Online Journal Material Science
ISSN: 2575-856X

Juniper PUBLISHERS key to the Researchers

Research Article
Volume 1 Issue 3 - May 2017
DOI: 10.19080/JOJMS.2017.01.555562

JOJ Material Sci

A Comparative Study of Carbon Anodes Produced by Ball Milling for Lithium-Ion Batteries

Tianchan Jiang* and M. Stanley Whittingham

Department of Chemistry, State University of New York, USA

Submission: April 04, 2017; **Published:** May 05, 2017

***Corresponding author:** Tianchan Jiang, Department of Chemistry, State University of New York, USA, Email: tjiang3@binghamton.edu

Abstract

The study of high energy density electrode materials is central to the development of lithium-ion batteries. With the goal to enhance the performance of lithium ion batteries in terms of anode, first, the currently dominating anode material graphite, a form of carbon, was investigated. Five different carbons in variable particle size and morphology were tested as electrodes and analyzed. Moreover, due to the increasing interest in nano-structured materials, nano crystalline graphite was formed after 1h, 5h and 10h of ball milling and included into the comparative study. Characterization techniques such as X-ray diffraction (XRD), scanning electron microscopy (SEM), and Raman spectrum have been utilized along with the electrochemical testing to understand correlations between the electro chemical performance and materials characteristics. Our results show that the rational control of morphology and composition plays a very important role in enhancing the electrochemical performance of graphite as anode for lithium-ion batteries.

Keywords: Graphite; Graphene; Carbon black; Carbon nanotube; Carbon anodes; Lithium ion batteries; Electrochemistry

Introduction

Lithium-ion batteries have attracted a vast amount of attention for their application in portable electronic devices and electric vehicles, etc. The practical anode materials that have been commercialized so far are carbonaceous compounds, mostly graphitic carbons, due to their capability for reversible lithium ion intercalation in the layered crystals. A large amount of research has been conducted on graphite and graphitic carbon during the last thirty years and the graphite in lithium intercalation compounds, LixC6 (0≤x≤1), has been investigated [1,2]. The intercalating lithium LiC_6 (x=1) is equivalent to a gravimetric specific capacity of 372mAh/g and a volumetric capacity of 1000mAh/cc below 0.3V vs. Li metal. Meanwhile, there has been increasing interest in nano crystalline grain size in the range of a few to a few tens of nanometers [3,4]. In both industrial and academic research fields, mechanical milling is a common approach that is widely used to mix precursors and facilitate solid-state reactions. During the milling process, particle size is reduced to as small as nano crycrystalline scale with reactants homogenously mixed. Furthermore, this method results in shrinking the diffusion paths for the solid-state reactions, thus the reaction time is saved. The mechanical milling technique has been used to prepare various nano structure materials, such as pure metallic substance [5,6] solid solutions [7] inter metallic compounds [5,6,8] and dispersion-strengthened alloys [9]. In this report, a comparative study was conducted on graphite produced by ball-milling to investigate structural disorder and consequent properties.

Other graphitized carbons with different host structures and textures such as graphene, single-walled and multi-walled carbon nano tubes, nano fibers, etc., opened up prospects for these materials and boosted activities in this field [9,10-12]. The electrical resistivity of graphite (in highly ordered pyrolytic graphite) is 0.04mΩ cm along the graphene sheets (sp^2-hybridized carbon atoms) and 150mΩ cm across the stacked graphene sheets, which indicates the small resistivity of a single crystal of graphite along the graphene sheet [13]. Since the paper on the freestanding graphene was reported by Novoselovet al. [14] increasing study of preparation, structure and property of graphene have been conducted. Given the high conductivity, surface area and aspect ratio, graphene is regarded as a promising candidate for the fabrication of anode and cathode in lithium ion batteries [15,16]. Theoretically, graphene can accommodate lithium ions on both sides of each sheet. The maximum capacity can be delivered as 740mAh/g in terms of LiC_3 instead of LiC_6 for natural graphite [1,2,17]. Further theoretical study using a Li2 covalent molecule model identified that the maximum amount of lithium insertion can be achieved with a capacity of 1116mAh/g in terms of LiC_6 [18]. Graphene is defined as a two-dimensional single carbon layer of graphite structure, describing its nature by analogy to a polycyclic aromatic hydrocarbon of quasi-infinite

size [19]. Nevertheless, this definition is usually deviated and the word "graphene" is used for a vast array of carbon materials, such as "graphene" can consist of single, few (two to nine layers), or even multiple layers (≥10 layers); in some cases, these multilayer graphenes can be called ultrathin graphite; another common deviation is heavily damaged graphene sheets with a crystallite size of nano meters, containing a large amount of sp_3-hybridized carbon defects, ad atoms, and physical holes in the structure with close resemblance to amorphous carbon [13].

Due to its unique morphology (e.g., helical or fishbone arrange of graphite layers, presence of a central canal, entanglement, bundles formation, etc.) and electronic properties, carbon nano tubes (CNT) have been considered to be profitable for getting improved performance. Multi-walled nano tubes/nano filaments (MWNTs) and single-walled nano tubes (SWNTs) have been used in electrodes, with the aim to obtain higher lithiation capability and better overall performance [20,21]. The currently accepted model for CNT is the "Russian doll" model, which shows graphitic sheets rolled into closed concentric cylinders with diameters on the order of nano meters and lengths on the order of micrometers [20-22]. When applied to lithium ion batteries, SWNT accommodates up to one lithium ion for every two or three carbon atoms to form LiC6 [9,10-12,20,21,23,24]

In most lithium ion batteries, carbon black (CB) has been used to improve electrical conductivity between the active materials [25]. It is also utilized as the anode material, since the irreversible process of a CB anode was addressed, [26] as well as the effects of its macroscopic structure on anode characteristics [27-29]. Capacity and electrochemical potential are key criteria for judging an anode candidate. In this report, based on structural investigations by x-ray diffraction, Raman scattering and scanning electron microscopy, we sought to study comparatively on graphite, graphene, carbon nano tubes and carbon black as anode materials for lithium ion batteries. In addition, the effect of structural disorder on electrochemical behavior in graphite and graphene is also investigated comparatively.

Materials and Methods

Four different carbons were studied, namely, graphite supplied by Sigma-Aldrich (powder, <20 micron, synthetic), graphene supplied by XG Sciences Co. (graphene: xGnP-C-750; multi-layered "graphene": xGnP-i Carbon black supplied by Timcal Ltd. (Super C65), and carbon nano tubes supplied by Sigma-Aldrich (Multi-Wall Carbon Nano tubes).

The ball milling was carried out in a conventional planetary ball mill as well as in a high-energy ball mill. For graphite, our goal is to investigate the ball mill effect, so a high-energy ball mill was used to maximize the change. Whereas for layered graphene, due to the large particle size of the pristine material, we used relatively gentle grinding-planetary ball mill and manual grinding, to grind the materials rather than destroy them, with the purpose of seeking good electrochemical performance. Pure graphite powder was put into a hard bearing steel vial and a high-energy ball mill was applied with a SPEX 8000D dual mixer/mill (SPEX Sample Prep LLC, USA). Graphene (multi-layered "graphene", xGnP-M-15) was ball milled using a planetary ball mill with a 4×100ml Gear-Drive 0.4L Planetary ball mill (Across International Co.).

The materials were characterized by X-ray diffraction (XRD) by Philips X'Pert MPD System, and the X-ray source tube uses a copper target (1.5418Å). The data were recorded during a step scan in the 2θ range of 10-60o. Scanning Electron Microscopy (SEM) characterized the morphology and elemental distribution, on a Zeiss Supra field emission scanning electron microscope operating at 10.0kV.

Electrochemical properties of these Si materials were evaluated in 2325-type coin cells under an argon atmosphere with cathode composite, a lithium anode, a Celgard 3501 separator, and a 1:1 volume mixture of ethylene carbonate and di-methyl carbonate (Novolyte) with 10% fluoro ethylene carbonate additive were tested on a VMP2 multi-channel potentiotat (Biologic) at C/40 rate (current density 0.12mA/cm^2) for the first cycle, followed by C/10 rate (0.5mA/cm^2) for the remaining cycles from 2.0V to 0.01V. The composites of the active material, carbon black (Timcal Ltd.) and sodium carboxy methyl cellulose (CMC, VMR) in a weight ratio of 70:20:10 were cast on copper foil, using a DI water slurry and dried at 85 °C in air for 12h. Capacities were calculated based on the weight of active mass (2-3mg/cm^2).

Result and Discussion

Physical characterization

Table 1: Lattice parameters of carbon samples.

Sample	FWHM (002 peak)	d_{002} (Å)
graphite	4.222	3.376
graphite_1h	4.236	3.364
graphite_5h	4.283	3.328
graphite_10h	4.305	3.311
graphene	4.263	3.345
G_NP	4.254	3.352
G_NP_15BM	4.260	3.347
G_NP_30BM	4.263	3.345
G_NP_30Manual	4.256	3.35
CB	4.009	3.546
CNT	4.207	3.387

The structural changes among graphite, graphene, layered graphene, carbon black (CB) and carbon nano tube (CNT) were investigated by XRD measurement, and the patterns are shown in Figure 1. The presence of (002) graphitic reflection in the XRD patterns indicates the characteristics of carbon. The lattice parameters are shown in (Table 1). The diffraction peaks corresponding to the (002) graphitic plane belong to the hexagonal phase, P63/mmc; 194, of graphitic carbon. The peak position appears at 2Θ=26.3-26.4, which is close to that of single

How to cite this article: Tianchan J, M. Stanley W. A Comparative Study of Carbon Anodes Produced by Ball Milling for Lithium-Ion Batteries. JOJ Material Sci. 2017; 1(3): 555561. DOI: 10.19080/JOJMS.2017.01.555562

crystalline graphite (2θ=26.5). This peak is different from turbo static graphite (2θ=25.8). These results clearly demonstrate that graphene materials possess a crystalline structure. The peak at around 44° is attributed to the (101) graphitic plane. The peak broadening may be attributed to the small particle size, and the height of the peak depends on the sample preparation as well as the XRD equipment settings. According to the Scherrer equation,

$$B(2\theta) = \frac{K\lambda}{L\cos\theta}$$

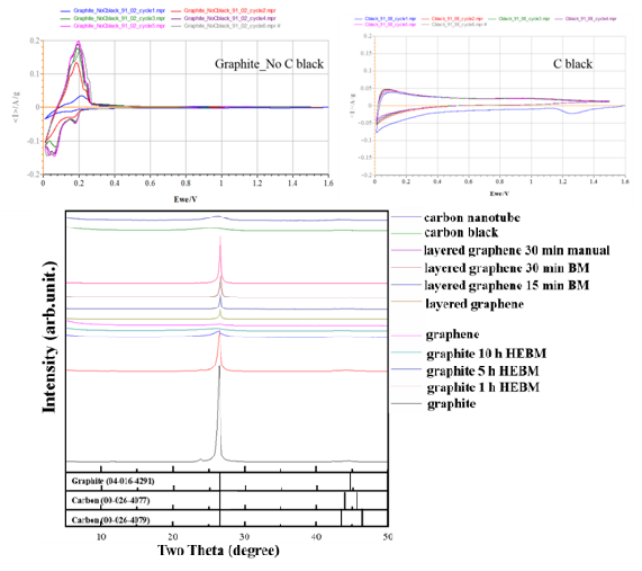

Figure 1: XRD patterns for the different carbon samples.

As stated in Chapter 2, peak width (B) is inversely proportional to crystallite size (L), namely, the crystallite size is larger when the peak is broader. In terms of ball mill (BM) factor, XRD patterns addressed the crystallite size difference of graphite series nicely: 10h ball-milled graphite<5h BM graphite 1h BM graphite<pristine graphite. The reason is clear to elucidate that ball milling process decreases the particle size by grinding big particles into small ones. However, it is another story for graphene series: graphene<layered graphene<layered graphene with 15min BM < layered graphene with 30 min BM <layered graphene with 30min manual grinding. Graphene possesses the smallest crystallite size, which may be due to its one-layer structure. Layered graphene is a deviation of graphene; the particles are still very small but with a few layers instead of one. In this regard, the case of ball mill factor in terms of graphene differs from that of graphite. Ball milling approach aggravates agglomeration for particles with small crystallite size, because there is no much potential to grind the particles into smaller pieces, and the dominant effect of the ball mill damages the structure. Therefore, the uniform and layered structure is destroyed and bonds are formed in a relatively random manner, thus the crystallite size increases.

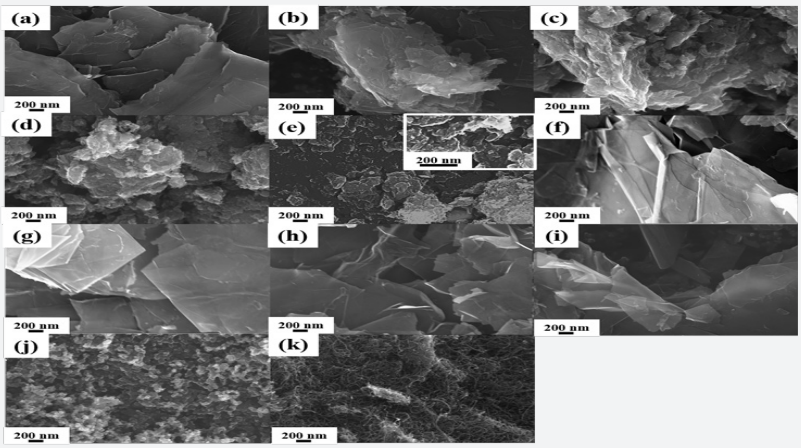

Figure 2: Structure of carbon materials under SEM showing (a) graphite, (b) to (d) graphite with 1h, 5h and 10h HEBM respectively, (e) graphene, (f) layered graphene, (g) (h) layered graphene with 15 and 30min BM respectively, (i) layered graphene with 30min manual grinding, (j) CB, (k) CNT.

How to cite this article: Tianchan J, M. Stanley W. A Comparative Study of Carbon Anodes Produced by Ball Milling for Lithium-Ion Batteries. JOJ Material Sci. 2017; 1(3): 555561. DOI: 10.19080/JOJMS.2017.01.555562

When comparing other carbon types, i.e. carbon nano tube (CNT) and carbon black (CB), with previously discussed graphite and graphene, CNT and CB demonstrates low peak height, indicating a relatively large crystallite size. The following SEM characterization may further illustrate this point. The morphology of these carbon materials was investigated by SEM, as shown in (Figure 2). From (Figure 2A-2D), pristine, un reacted graphite crystalline and smooth sheets. As the ball-milling time increases, its walls tended to be rough and broke into small particles. Gradually losing its original intact sheet morphology, the graphite after 10 h HEBM treatment had highly aggregated particles with roughly textured sidewalls. In terms of the two kinds of graphene, the structural morphology was revealed in (Figure 2E-2I). All the layered graphene materials (Figure 2F-2I) were crystalline with smooth sheets, while the fine graphene (Figure 2 E) present small and random-shaped flakes stacking on larger flakes, and agglomerates were observed. Such structure remains the same under high magnifications, as shown in the inset of (Figure 2E). In terms of the other two carbon types, CB displayed small granular particles with a size of ~40 nm, which is consistent with the data from the supplier; and CNT demonstrated long and tubular morphology, as expected.

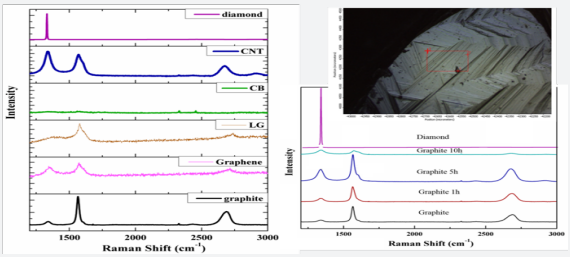

Figure 3: Raman spectra of carbon materials. The inset is the area selected on diamond for Raman characterization.

Raman spectroscopy has emerged as one of the most convenient techniques for characterizing graphene materials in a nondestructive way to provide information on structural features, density of defects, and the number of graphene layers. It functions on the basis of analyzing the scattering of monochromatic light that interacts with molecular vibrations and phonons of a particular solid. It has been used extensively to characterize carbon materials that show significant and characteristic Raman features in the region of 1200-3000cm−1 of Raman shift. The Raman spectra of the carbon series are shown in (Figure 3). The area selected on diamond carbon was shown as the inset in (Figure 3).

Table 2: Details of the observed peaks in Raman spectra - Intensity ratios.

Carbon Type	Raman Peak Intensity Ratio			Raman peak position (cm-1)		
	R=ID/IG	R'=ID/IG'	RG=IG/ IG'	D	G	G'
Graphite	0.113	0.240	2.130	1341.81	1565.51	2686.92
Graphite 1h HEBM	0.221	0.403	1.823	1340.85	1564.27	2684.99
Graphite 5h HEBM	0.442	0.935	2.115	1337.96	1566.48	2679.20
Graphite 10h HEBM	1.154	3.813	3.304	1341.81	1572.26	2681.13
Graphene	0.885	1.111	1.256	1345.16	1574.16	2696.87
Layered Graphene	0.663	0.941	1.418	1385.21	1578.34	2696.87
CB	0.724	8.324	11.504	1363.03	1559.73	2654.13
CNT	1.143	2.443	2.137	1338.92	1569.37	2675.35

*The positions of D-band, G-band and G' band peaks are at ~1350, ~1580 and ~2700 cm-1 respectively.

The signature bands of the Raman spectra of graphite and graphene are the G band at ~1584 cm^{-1} and the G' band at ~2700cm-1. The G band is due to the in-plane E_{2g} vibrational mode of sp^2-bonded carbons. The G' (also dominated as 2D) band is attributed to the second-order two-phonon mode [30], and this band changes substantially in relation to the quality and number of graphene layers. A third feature, the D band at ~1360 cm^{-1}, is not Raman active for pristine graphene but can be observed where symmetry is broken by edges or in samples with a high density of defects. The D band is generated by the out-of-plane vibrations of sp^2 carbon atoms, but it is active only in the presence of defects (edges, sp^3 carbons, vacancies, adatoms, etc.). In addition, a weak D' peak at about 1620 cm^{-1} is observed in the presence of disorders. A legend method to distinguish the type of disorder present in graphene has been proposed on the basis of analyzing the intensity ratio between the D and D' bands, whereas this ratio is not often valid due to the weak intensity of the D' peak. The peak at 1332cm^{-1} is associated with defects of sp^3, which is characteristic for diamond carbon. The details of the Raman spectra of the carbon materials including the peak position and intensity ratio are given in (Table 2).

There are three ratios, R, R' and R_G, based on the intensity of the observed peaks, are usually used as indicators. The ratio R, R' and RG are defined as I_D/I_G, I_D/I_G' and IG/IG', respectively. As found by Tuinstra and Koeninget.al, the ratio R is inversely proportional to the effective crystallite size in the direction of the graphite plane L_a, where L_a=4.4/R [21]. Due to the curved nature of graphite layers in carbon nano tubes, the empirical formula of La may not be applicable for CNT analysis. However, the value of

How to cite this article: Tianchan J, M. Stanley W. A Comparative Study of Carbon Anodes Produced by Ball Milling for Lithium-Ion Batteries. JOJ Material Sci. 2017; 1(3): 555561. DOI: 10.19080/JOJMS.2017.01.555562

R remains valid. [9,32] According to the R value shown in (Table 2), R value increases as ball mill time increases, which implies the increment of crystallite size. This result is consistent with other reports involving ball mill effect on graphite, [33] and it also matches the results of the previously discussed XRD analysis. Another ratio R', namely, ID/IG'¬, has been taken as an indicator of the extent of defects in the structure. [30,31] In terms of the factor of ball milling, R' value shows that more ball milling results in more defects. Comparing in terms of different carbon types, the order of increasing defects may be arranged as graphite < layered graphene< CB <graphene< CNT. The peak positions and the relative peak heights of the G and G' bands indicate the number of layers present for a given flake. The location of the G peak for single layer graphene is 3-5cm^{-1} higher than that for bulk graphite, while its intensity is roughly the same. A single graphene sheet generates a sharp G' band, which is roughly four times more intense than the G band. Upon increasing the number of graphene layers up to five layers, the G' band decreases in intensity, splits into multiple sub-peaks, and shifts toward higher wave numbers up to 5cm^{-1}. The G' peak shows a significant change in both shape and intensity as the number of layers decreased. In bulk graphite, the G band is comprised of two components, the intensities of which are roughly 1/4 and 1/2 that of the G peak for the low and high shift, respectively. For single layer graphene, the G' band is a single sharp peak at the lower shift, with intensity roughly 4 times that of the G peak. It was following these trends that finally enabled scientists to reliably confirm the identity of mechanically exfoliated flakes [30]. Relative peak heights of the G and G' bands (RG) indicate the number of layers present for a given flake. Namely, the value of RG increases, the number of graphite layers increases. Raman spectrum of graphene consisting of more than five layers is hardly distinguishable from that of graphite. Besides Raman scattering, Rayleigh scattering has also been proposed to characterize graphene materials with a possibility to distinguish up to six layers of graphene sheets.

Electrochemical Properties

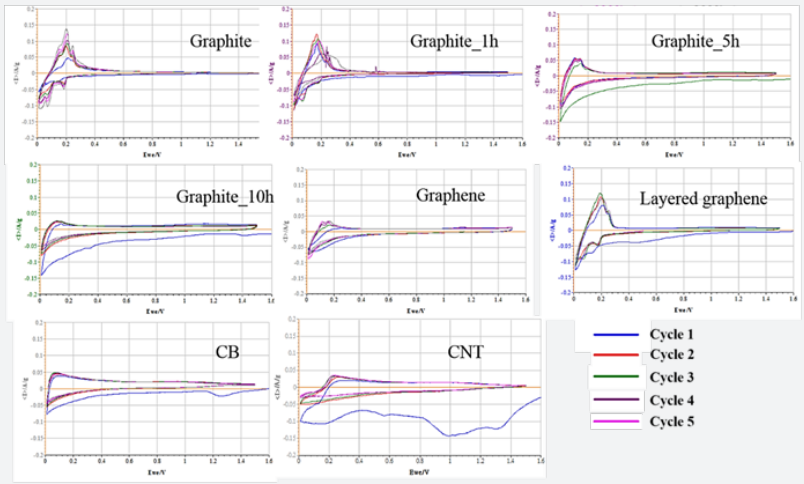

Figure 4: Cyclic voltammogram of carbon materials.

The cyclic voltammograms of the pristine untreated graphite along with the graphite treated with 1h, 5h and 10h HEBM are shown in (Figure 4) [32,33]. Characteristics of graphite appeared to be weak when high-energy ball milling treatment was applied, and the 10 h BM graphite was almost inactive as observed. The main redox peaks occur at around 0.20, 0.10, and 0.02 V for the reduction during cathodic scans, and at around 0.25, 0.20, and 0.15 V for the corresponding oxidation during anodic scans, respectively. These peaks are the characteristic LiC_x phase transformation peaks that are observed during lithiation and de-lithiation processes as reported in the literature [34-36]. The broad peak at 0.85 V corresponds to the initial formation of an SEI layer by the irreversible decomposition of electrolyte components at graphite surfaces. No other new peaks from HEBM have been observed, however some peaks are weakening due to loss of their characteristics, which is consistent with their structural change examined by XRD and SEM techniques. It is observed that graphite anode with 1 h HEBM does not change the bulk graphite material much and possesses the same basic electrochemical characteristics as the milling-free graphite which can be confirmed from its CV scan curves. However, it is found that a lower current density is achieved by the milled graphite anodes, probably because the ion conductive resistance of the SEI layer formed on the milled graphite is lower than that of the SEI layer formed on the un milled graphite [34-37] Comparing the CV curves for graphene, layered graphene and graphite at the scan rate of 0.2 mV/s, the characteristic peaks for graphite are also clearly revealed. Graphene curves are largely diminished, the low current resulting from high ion conductive resistance due to the large amount of defects from its single layer structure. At the sixth cycle of the three materials, this behavior is confirmed once more. The layered graphene possesses almost

How to cite this article: Tianchan J, M. Stanley W. A Comparative Study of Carbon Anodes Produced by Ball Milling for Lithium-Ion Batteries. JOJ Material Sci. 2017; 1(3): 555561. DOI: 10.19080/JOJMS.2017.01.555562

the same property as normal graphite, despite some impact on its current, the overall feature maintained. Whereas for graphene, the characteristic features, especially redox peaks, have almost vanished. In terms of the CV curves for CB and CNT, the peak corresponding to the 1V plateau, where lithium was removed, during the charge is apparent for CNT, but not apparent for CB.

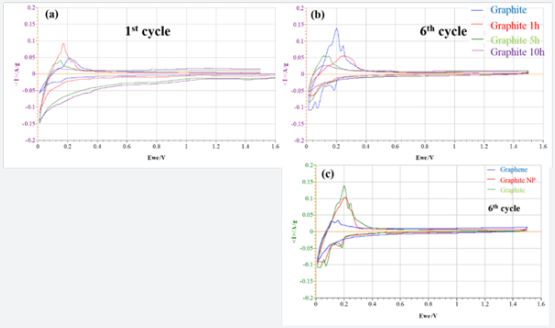

Figure 5: Cyclic voltammetry curves of (a) the 1st and (b) 6th cycle for the graphite series; (c) the 6th cycle for graphene, layered graphene(Graphite NP) and graphite on the bottom (scan rate: 0.2 mV/s).

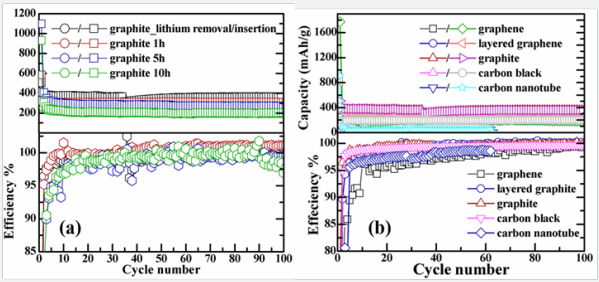

Figure 6: Electrochemical performance of (a) graphite with different ball mill treatment, and (b) different carbon materials.

The 1st and 6th cycle of cyclic voltammograms for the pristine, untreated graphite along with the graphite treated with 1h, 5h and 10h HEBM are shown in Figure 5A & 5B, and the 6th cycle for graphene, layered graphene and graphite is plotted in Figure 5C. The voltammograms reflect an irreversible cathodic wave at the first cycle that belongs to the reduction and passivation processes and their highly reversible repeated Li insertion into the electrodes. As mentioned before, the current reflects resistance. In this regard, the ion conductive resistance of the SEI layer decreases after the layer has been formed after the first cycle, and the ion conductive resistance is high for the milling treated graphite due to pulverization of the structure. Both Figure 4&5 are based on the CV tests at 0.2 mV/s scan rate (Figure 6A) demonstrates the electrochemical performance for the graphite currently used in lithium battery anodes along with the same graphite after 1 h, 5 h and 10 h high-energy ball milling with the same electrode composition. In 100 cycles the graphite with HEBM treatment shows lower capacity than the pristine, untreated graphite. The capacity maintains at 360 mAh/g for pristine graphite anode up to 100 cycles, while the capacity is lowered to 313, 269 and 196 mAh/g for the graphite products with 1 h, 5 h and 10 h milling, respectively. The cycle ability in terms of efficiency also indicates the same trend. As shown in Table 1, the first cycle efficiency reaches 74.8% for pristine graphite, while it drops to 56.5%, 37.3% and 34.7% for the graphite products with 1 h, 5 h and 10 h milling, respectively. The electrochemical behavior was all carried out as C/30 rate for the first formation cycle, followed by C/15 rate for the following cycles.

Electrochemical performance of different carbon materials was investigated, as shown in (Figure 6B). Among graphite, graphene and layered graphene, graphite possesses the best cycling stability, maintaining a capacity of 360 mAh/g, whereas layered graphene demonstrates 254 mAh/g and graphene has 183mAh/g after 100 cycles. The columbic efficiency can be reached as high as 99.5% for graphene after 100 cycles, and 99.9%, 99.7% for graphite NP and graphite, respectively. First cycle efficiency, as shown in table 3, is as low as 17.8% for graphene due to its structural feature, most of the lithium failed to get out after inserting into the layers. The capacity of CB and CNT are relatively low as well as their columbic efficiency, especially in the case of CNT, which fades rapidly and drops to a very low capacity in the first several cycles.

Table 3: First cycle efficiency of carbon materials in different types.

Carbon Types	First Cycle Efficiency %
Graphite	74.8
Graphite 1h HEBM	56.5
Graphite 5h HEBM	37.3
Graphite 10h HEBM	34.7
Graphene	17.8
Layered Graphene	43.2
CB	52.5
CNT	6.1

Carbon black influence on graphite

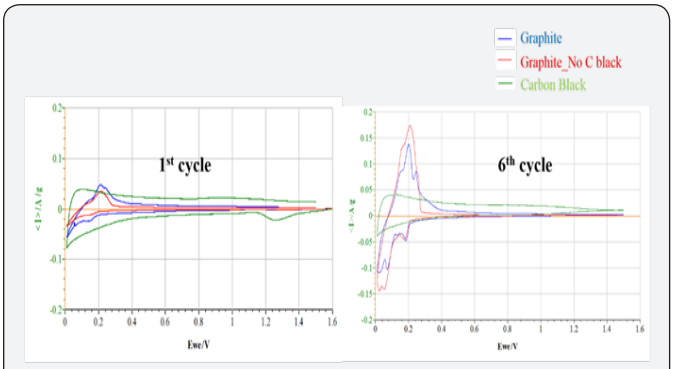

Figure 7: Cyclic voltammetry curves of graphite without carbon black electrode, and carbon black only electrode, and the cyclic voltammetry curves at 1st and 6th cycle (scan rate: 0.2 mV/s).

A typical electrode is usually composed of ~80% active material, 10% CB and 10% binder by weight. However, considering graphite and CB are both a form of carbon, graphite electrode without adding CB was studied to investigate the CB

How to cite this article: Tianchan J, M. Stanley W. A Comparative Study of Carbon Anodes Produced by Ball Milling for Lithium-Ion Batteries. JOJ Material Sci. 2017; 1(3): 555561. DOI: 10.19080/JOJMS.2017.01.555562

impact. The cyclic voltammetry curves are shown in (Figure 7). The graphite electrode contains 80% graphite, 10% carbon black and 10% CMC binder by weight, while the graphite without carbon black electrode comprises 90% graphite and 10% CMC, and carbon black electrode is made of 90% carbon black and 10% CMC by weight.

As mentioned in the discussion of Figure 4, the characteristic peaks for graphite are clearly shown in the graphite without carbon black curve. The main redox peaks occur at around 0.20, 0.10, and 0.02 V for the reduction during cathodic scans, and at around 0.25, 0.20, and 0.15 V for the corresponding oxidation during anodic scans, respectively. These peaks are the characteristic LiCx phase transformation peaks that are observed during lithiation and de-lithiation processes, whereas carbon black curves are apparently not active, which presents very low current resulting from high ion conductive resistance. The first cycle CV curves show low current achieved by all the three composites, while similar peaks were observed in the CV curves of graphite electrode and graphite without carbon black electrode; the current achieved is low due to the resistance caused by SEI layer formation. At the 6th cycle, however, the current grows high and all the characteristic peaks are clearly shown after the SEI layer formed. Carbon black curves remained inactive through the first cycle to the 6th cycle with no significant peaks observed.

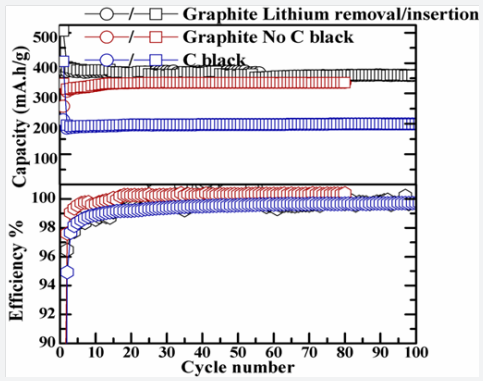

Figure 8: Electrochemical data of graphite electrode, graphite without carbon black electrode, and carbon black only electrode.

The capacity versus cycle number curves for the graphite electrode, carbon black free graphite electrode and carbon black only electrode are shown in Figure 8. The observed capacity after 100 charging/discharging operations was 360 mAh/g, 336 mAh/g and 199 mAh/g for graphite, carbon black free graphite and carbon black only electrodes, respectively (Table 4) illustrates the first cycle efficiency of the three electrodes with different compositions, graphite anode with 10% carbon black delivered a first cycle efficiency of 74.8%, while the graphite only electrode gives 73.1% and carbon only electrode gives 52.5%. This implies that carbon black is not the major reason for the efficiency fading of the graphite electrode, since the graphite-only electrode shows an even higher first cycle loss. The corresponding coulombic efficiency was given at 99.7%, 98.8% and 99.7% until 100 cycles. In this regard, carbon black may not be removed from the graphite anode electrode, even though they are both carbon (Table 5).

Table 4: First cycle efficiency of graphite electrode, graphite without carbon black electrode, and carbon black only electrode.

Materials	Graphite Electrode with 10% CB	Graphite Electrode with No CB	CB
First cycle efficiency %	74.8	73.1	52.5

Table 5: Abbreviations.

Abbreviation	Defination
G_NP	Grapheme nanoparticle
BM	Ball-milling
HEBM	High-energy ball-milling
CB	Carbon black
CNT	Carbon nanotube

Conclusion

Our results show that the rational control of morphology and composition plays a critical role in enhancing the electrochemical performance of carbon as anode in lithium-ion batteries. Ball milling does not have a positive effect on the electrochemical behaviour. Graphite displayed the best cyclability. The dominating reason may be its layered morphology, which could effectively and reversibly intercalate and deintercalate lithium. Carbon black plays a significant role in electrode composition.

References

1. Dahn JR, Zheng T, Liu YH, Xue JS, (1995) Mechanisms for lithium insertion in carbonaceous materials. Science 270(5236): 590-593.
2. Winter M, Besenhard JO, Spahr ME, Novak P (1998) Insertion electrode materials for rechargeable lithium batteries. Advanced Materials 10(10): 725-763.
3. Gleiter H (1989) Nano crystalline Materials. Progress in Materials Science 33(4): 223-315.
4. Gryaznov VG, Trusov LI (1993) Size effects in micromechanics of nano crystals. Progress in Materials Science 37(4): 289-401.
5. Wang KY, Shen TD, Quan MX, Wei WD (1993) Hall-Petch relationship in nano crystalline titanium produced by ball-milling. Journal of Materials Science Letters 12(23): 1818-1820.
6. Hellstern E, Fecht HJ, Fu Z, Johnson WL (1989) Structural and thermodynamic properties of heavily mechanically deformed ru and airu. Journal of Applied Physics 65(1): 305-310.
7. Klassen T, Oehring M, Bormann R (1994) The early stages of phase-formation during mechanical alloying of ti-al. Journal of Materials Research 9(1): 47-52.
8. Aoki K, Itoh Y, Masumoto T (1994) Preparation of nano crystalline tial powder by the hddr process using mechanical grinding in a hydrogen atmosphere. Scripta Metallurgica Et Materialia 31(9): 1271-1275.
9. Wu GT, Wang CS, Zhang XB, Yang HS, Qi ZF He et al. (1999) Structure and lithium insertion properties of carbon nano tubes. Journal of the Electrochemical Society 146(5): 1696-1701.

How to cite this article: Tianchan J, M. Stanley W. A Comparative Study of Carbon Anodes Produced by Ball Milling for Lithium-Ion Batteries. JOJ Material Sci. 2017; 1(3): 555561. DOI: 10.19080/JOJMS.2017.01.555562

10. Schollhorn R, Payer A (1985) Cis-Tis2, A New modification of titanium disulfide with cubic structure. Angewandte Chemie-International Edition in English 24(1): 67-68.

11. Zhang Y, Ichihashi T, Landree E, Nihey F, Iijima S (1999) Heterostructures of single-walled carbon nanotubes and carbide nanorods. Science 285(5434): 1719-1722.

12. Bai LZ, Zhao DL, Zhang TM, Xie WG, Zhang JM et al. (2013) A comparative study of electrochemical performance of graphene sheets, expanded graphite and natural graphite as anode materials for lithium-ion batteries. Electrochimica Acta 107: 555-561.

13. Ambrosi A, Chua CK, Bonanni A, Pumera M (2014) Electrochemistry of graphene and related materials. Chem Rev 114(14): 7150-7188.

14. Novoselov KS, Geim AK, Morozov SV, Jiang D, Zhang Y et al. (2004) Electric field effect in atomically thin carbon films. Science 306(5696):666-669.

15. Geim AK, Novoselov KS (2007) The rise of graphene. Nat Mater 6(3): 183-191.

16. Han S, Wu DQ, Li S, Zhang F, Feng XL (2013) Graphene: A Two-Dimensional platform for lithium storage. Small 9(8): 1173-1187.

17. Liu C, Li F, Ma LP, Cheng HM (2010) Advanced materials for energy storage. Adv Mater 22(8): E28-E62.

18. Sato K, Noguchi M, Demachi A, Oki N, Endo M (1994) A Mechanism of lithium storage in disordered carbons. Science 264(5158): 556-558.

19. Fitzer E, Kochling KH, Boehm HP, Marsh H (1995) Recommended terminology for the description of carbon as a solid - (Iupac Recommendations 1995). Pure and Applied Chemistry 67(3): 473-506.

20. Frackowiak E, Beguin F (2002) Electro chemical storage of energy in carbon nano tubes and nano structured carbons. Carbon 40(10): 1775-1787.

21. Jana M, Sil A, Ray S (2014) Morphology of carbon nanostructures and their electrochemical performance for lithium ion battery. Journal of Physics and Chemistry of Solids 75(1): 60-67.

22. Ajayan PM, Iijima S (1992) Smallest carbon nanotube. Nature 358(6381): 23-23.

23. Zhao J, Buldum A, Han J, Lu JP (2000) First-principles study of Li-intercalated carbon nano tube ropes. Physical Review Letters 85(8): 1706-1709.

24. Lee DH, Kim DW, Park JG (2008) Enhanced Rate Capabilities of Nano brookite with Electronically Conducting MWCNT Networks. Crystal Growth & Design 8(12): 4506-4510.

25. Fransson L, Eriksson T, Edstrom K, Gustafsson T, Thomas JO (2001) Influence of carbon black and binder on Li-ion batteries. Journal of Power Sources 101(1): 1-9.

26. Takei K, Kumai K, Iwahori T, Uwai T, Furusyo M (1993) Carbon-Black as an anode material in lithium secondary cells - effects of heat-treatment on the electrochemical behaviors. Denki Kagaku 61(4): 421-430.

27. Takei K, Terada N, Kumai K, Iwahori T, Uwai T, Miura T (1995) Effects of the macroscopic structure of carbon-black on its behavior as the anode in a lithium secondary cell. Journal of Power Sources 55(2): 191-195.

28. Sleigh AK, Vonsacken U (1992) Unusual cycling behavior of disordered carbons in Li/C Cells. Solid State Ionics 57(1-2): 99-102.

29. Li GB, Xue RJ, Chen LQ, Huang Y (1995) Carbon electrode materials for lithium-ion batteries. Journal of Power Sources 54(2): 271-275.

30. Allen MJ, Tung VC, Kaner RB (2010) Honeycomb Carbon: A Review of Graphene. Chemical Reviews 110(1): 132-145.

31. Tuinstra F, Koenig JL (1970) Raman spectrum of graphite. The Journal of Chemical Physics 53(3): 1126-1130.

32. Kastner J, Pichler T, Kuzmany H, Curran S, Blau W, et al. (1994) Resonance Raman and infrared spectroscopy of carbon nanotubes. Chemical Physics Letters 221(1-2): 53-58.

33. Shen TD, Ge WQ, Wang KY, Quan MX, Wang JT, et al. (1996) Structural disorder and phase transformation in graphite produced by ball milling. Nano structured Materials 7(4): 393-399.

34. Levi MD, Aurbach D (1997) The mechanism of lithium intercalation in graphite film electrodes in aprotic media .1. High resolution slow scan rate cyclic voltammetric studies and modeling. Journal of Electro analytical Chemistry 421(1-2): 79-88.

35. Zhang SS, Ding MS, Xu K, Allen J, Jow TR (2001) Understanding solid electrolyte interface film formation on graphite electrodes. Electrochemical and Solid State Letters 4(12): A206-A208.

36. Ding F, Xu W, Choi D, Wang W, Li X, et al. (2012) Enhanced performance of graphite anode materials by AlF3 coating for lithium-ion batteries. Journal of Materials Chemistry 22(25): 12745-12751.

37. Lee DJ, Lee KS, Myung ST, Yashiro H, Sun YK (2011) Improvement of electrochemical properties of Li(1.1)Al(0.05)Mn(1.85)O_4 achieved by an AlF_3 coating. Journal of Power Sources 196(3): 1353-1357.

DOI: 10.19080/JOJMS.2017.01.555562

How to cite this article: Tianchan J, M. Stanley W. A Comparative Study of Carbon Anodes Produced by Ball Milling for Lithium-Ion Batteries. JOJ Material Sci. 2017; 1(3): 555561. DOI: 10.19080/JOJMS.2017.01.555562